Response to Reviewers

Dear editor and reviewers:

Thank you very much for your letter and the constructive comments concerning our manuscript, now entitled "*Impacts of synoptic circulation types on nocturnal ozone increase in the North China Plain: Meteorological drivers and physical mechanisms*" (Manuscript ID: egusphere-2026-25).

We deeply appreciate the time and effort you have dedicated to reviewing our work. The insightful feedback has been exceedingly valuable in refining our terminology, strengthening our scientific arguments, and improving the overall quality of the paper. We have carefully considered all the comments and revised the manuscript accordingly.

General Update: Please note that to ensure absolute terminological rigor and to perfectly align with the reviewers' excellent suggestions, we have slightly adjusted the title from "...formation mechanisms" to "...physical mechanisms".

Please find below our detailed point-by-point responses to the specific comments as follows:

Reviewers' comments are in black.

Authors' responses are in blue.

Changes in the manuscript are in red.

Your Sincerely,

Liya Fan,

On behalf of the authors

Reviewer #3

Methodological Issues:

1. NOI significance is not addressed. The definition of a NOI event does not account for baseline ozone levels. An increase of 10 ug/m^3 over a baseline of 70 ug/m^3 is not equivalent to the same increase over 120 ug/m^3. Similarly, the temporal trajectory matters: a 10 ug/m^3 rise followed by an immediate decline is fundamentally different from a sustained or accelerating increase. These dimensions must be incorporated into the event detection framework.

Response 1: Thanks for reviewer's comments. We rigorously re-evaluated our event detection framework. We ultimately retained the standard >10 μg m^{-3} per hour absolute increment threshold, but we realized that our original manuscript failed to explicitly articulate why this choice was deliberately made to serve the specific dynamic focus of this study. We have now addressed this extensively in the revised text based on the following scientific rationales:

(1) Using absolute increment as a pure proxy for physical transport: The core objective of this study is to unravel the synoptic-scale meteorological drivers (e.g., strong wind shear, regional subsidence) that physically break the nocturnal inversion. From a fluid dynamics perspective, a sudden hourly surge of >10 μg m^{-3} indicates that a rapid, massive downward or horizontal physical transport has abruptly overpowered the local nocturnal depletion (titration and deposition). This absolute increment acts purely as a mathematical proxy for the mechanical transport, independent of the background chemical baseline. This absolute increment threshold is currently the widely accepted standard in meteorological NOI studies (Zhu et al., 2020; He et al., 2022; Wang et al., 2025; Wang et al., 2023b).

(2) Clarifying the significance of NOI in the revised text: To ensure readers do not conflate our physical detection metric with a health exposure assessment, we have expanded our narrative:

In the revised Introduction: We now discuss the broad significance of NOI regardless of the initial baseline. We clarified that these nocturnal intrusions critically elevate the surface baseline for the following morning (exacerbating next-day photochemical smog) and fundamentally alter the nocturnal atmospheric oxidative capacity (AOC) by fueling NO_3 and N_2O_5 chemistry.

In the revised Methodology (Section 2.2): We have added a dedicated paragraph explicitly defining the scope of this study. We acknowledge that while baseline is crucial for exposure

assessments, the absolute hourly increment is maintained as a robust indicator for detecting the timing and occurrence of pure meteorological physical intrusions.

Lines 43-55:

NOI events, characterized by unexpected rises in nighttime O_3 concentrations (at least 10 μg m^{-3} per hour (Zhu et al., 2020)), challenge the conventional understanding of O_3 (Wang et al., 2023b; Xue et al., 2023; Chen et al., 2024b). Previously, nocturnal O_3 was often overlooked owing to its low concentrations. Although a quantitative threshold of a 10 μg m^{-3} hourly increase may appear modest during a clean night, the scientific and environmental significance of NOI episodes extends far beyond simple numerical detection. First, NOI events can occasionally result in a rapid surge in nighttime O_3 levels surpassing 160 μg m^{-3} (Wang et al., 2023b; Zhu et al., 2024), directly posing nocturnal threats to human health and plant stomatal uptake (Chowdhury et al., 2022; Hoshika et al., 2019). More critically, even when absolute concentrations remain moderate, the horizontal or vertical transport of O_3-rich air that typically triggers NOI significantly elevates the surface O_3 baseline for the following morning. This higher initial baseline accelerates daytime accumulation, effectively exacerbating subsequent daytime photochemical smog (Wang et al., 2025). Furthermore, unexpected nighttime O_3 increments fundamentally alter the nocturnal atmospheric oxidative capacity (AOC). The enhanced O_3 facilitates dark reactions with nitrogen dioxide (NO_2) to generate nitrate radicals (NO_3) and dinitrogen pentoxide (N_2O_5), critical precursors for particulate nitrate and secondary organic aerosols (SOA), thereby linking NOI directly to regional fine particulate matter ($PM_{2.5}$) pollution (Wang et al., 2023a).

Lines 116-125:

NOI event is defined as an hourly O_3 concentration increment exceeding 10 μg m^{-3} during nighttime (20:00-06:00 local time, LT; UTC+8, Beijing Time) (He et al., 2021; Zhu et al., 2020). This absolute increment threshold is widely adopted in current literature (Zhu et al., 2024; Zhu et al., 2020; He et al., 2022; Wang et al., 2025) because it acts as an indicator for detecting the abrupt physical intrusion of O_3-rich air masses into local surface. While the absolute baseline concentrations and temporal trajectories of O_3 are crucial for evaluating human health exposure and long-term air quality attainment, the primary objective of this study is to isolate the underlying synoptic and meteorological transport mechanisms. Regardless of the initial surface baseline, a

sudden hourly surge of >10 μg m^{-3} effectively and consistently flags that sudden dynamic transport processes (whether via robust horizontal advection, massive vertical subsidence, or other regional intrusions) have completely overpowered the steady local nocturnal depletion (e.g., NO titration and dry deposition). Therefore, this increment-based metric provides the most robust and objective foundation for our dynamical and meteorological analysis.

2. The separation of night and morning periods is not adequately justified. While the intent is presumably to identify isolated days, this artificial split breaks the continuity of nocturnal dynamics. An increase beginning at night may well persist or evolve into the morning hours, and this continuity is lost under the current approach.

Response 2: Thanks for reviewer's comments. To address this exact issue and preserve the unbroken evolution of nocturnal transport, we have revised our temporal definition in the revised manuscript (Section 2.2).

Instead of an artificial calendar-day split, our event detection framework now treats the physical night as a single, continuous process. As stated in the revised text: "Since nighttime generally lasts from 20:00 to 06:00 LT the next day, it constitutes a continuous process. Therefore, a day is classified as an NOI day if such events occur from 20:00 to 06:00 LT the next day. By strictly confining the concept of NOI days to this continuous nocturnal window, we ensure that our dynamic analysis remains completely isolated from daytime photochemical interference." (Note: The morning cut-off is physically mandated by local sunrise to strictly prevent daytime contamination, and not to artificially break nocturnal continuity).

Under this revised continuous framework, an event that begins in the early night and persists into the morning hours is successfully captured as a single, uninterrupted event. Furthermore, to statistically describe when these events occur within this continuous night without using arbitrary mathematical intervals, we introduced three types that perfectly align with the physical evolution phases of the nocturnal boundary layer: (1) Early-night NOI (EN): The event occurs only between 20:00 and 23:00 LT, corresponding to the transitional boundary layer phase; (2) Late-night NOI (LN): The event occurs only between 00:00 and 06:00 LT, corresponding to the highly stable surface inversion phase; (3) Whole-night NOI (WN): The event occurs across both periods, persisting continuously through the night. These three sub-categories carry no other complex

implications, and they serve strictly as statistical labels.

Lines 126-137:

Considering the seasonal variation in local sunrise time, we excluded NOI events occurring after 05:00 LT from April to September, when the sunrise occurs relatively early. Since nighttime generally lasts from 20:00 to 06:00 LT the next day, it constitutes a continuous process. Therefore, a day is classified as an NOI day if such events occur from 20:00 to 06:00 LT the next day (excluding April to September, for which the window is 20:00 to 05:00 LT). By strictly confining the concept of NOI days to this continuous nocturnal window, we ensure that our dynamic analysis remains completely isolated from daytime photochemical interference. To further investigate the temporal occurrence characteristics within this continuous night, we subsequently categorized these NOI days into three descriptive types. Rather than using arbitrary mathematical intervals, the specific timeframes for these types were chosen to perfectly align with the distinct physical evolution phases of the nocturnal boundary layer: (1) Early-night NOI (EN): The event occurs only between 20:00 and 23:00 LT, corresponding to the transitional boundary layer phase; (2) Late-night NOI (LN): The event occurs only between 00:00 and 06:00 LT, corresponding to the highly stable surface inversion phase; (3) Whole-night NOI (WN): The event occurs across both periods, persisting continuously through the night.

3. The HYSPLIT methodology is described too briefly to be reproducible. As written, it would not allow an independent researcher to replicate the analysis. Furthermore, the Concentration-Weighted Trajectory (CWT) approach receives no methodological explanation whatsoever.

Response 3: Thanks for reviewer's comments. To ensure complete transparency and reproducibility, we have expanded Section 2.4 in the revised manuscript:

(1) Reproducibility of the HYSPLIT model: We have added the missing specific parameters required for independent replication. The revised text now explicitly details the spatial resolution of the GDAS data (1° × 1°), the temporal resolution of the trajectory calculations (at 1-hour intervals during the events), and clarifies the model execution environment.

(2) Methodological explanation of CWT: While the complete mathematical equations and weighting functions (W_{ij}) for the CWT approach were provided in Text S1 in the original

submission, we realize that a clear conceptual summary was missing from the main text. We have now incorporated a dedicated paragraph in Section 2.4 explaining the methodological mechanism of CWT. Specifically, how it calculates weighted average concentrations across grid cells to identify upwind source contributions, and how the empirical weighting coefficient mitigates uncertainties. We have also made the reference to the mathematical formulas in Text S1 much more prominent.

Lines 164-178:

The hybrid single particle lagrangian integrated trajectory (HYSPLIT) is a common model for investigating meteorological transmission channels (Chen et al., 2024; Cheng et al., 2024; Shi et al., 2024; Stein et al., 2015). It can efficiently and accurately determine the transport trajectories of different pollutants, classify and aggregate the backward trajectories during the study period through the Euler clustering method, and output air mass trajectories with different proportions. In this study, the HYSPLIT model (run via the TrajStat plugin / MeteoInfo) was used to identify backward trajectories for Xinxiang during the period from 2021 to 2023. The model inputs hourly meteorological data from the Global Data Assimilation System with a spatial resolution of 1° × 1° (ftp://arlftp.arlhq.noaa.gov/pub/archives/gdas1). Taking the starting point (central location of Xinxiang: 35.30°N, 113.88°E) as a reference, 48-hour backward trajectories terminating at 100 m above ground level were calculated at 1-hour intervals for all identified representative NOI days. Using these air mass trajectories, we mapped O_3 concentrations to specific geographic grids to apply Concentration-Weighted Trajectory (CWT) analysis. Briefly, the CWT approach calculates the weighted average concentration of air mass trajectories passing through each 1° × 1° grid cell, thereby quantitatively identifying the relative contributions of potential upwind source regions to local O_3 spikes (Shi et al., 2024; Wang et al., 2024). To mitigate statistical uncertainties from grid cells with sparse trajectory endpoints, an empirical weighting function W_{ij} was incorporated. The complete mathematical formulations and calculation parameters for the CWT methodology are detailed in Text S1.

4. The weather type classification lacks transparency. The identification and classification methodology appears highly subjective in its current description.

Response 4: Thanks for reviewer's comments. In the original manuscript, the aggregation of the detailed Lamb-Jenkinson (L-J) weather types into the four primary archetypes (A, C, S, and WNE)

was described too briefly, which may have given the impression of a subjective clustering approach.

To eliminate any subjectivity and ensure total transparency, we have fundamentally reconstructed the classification methodology in the revised manuscript. As detailed in the extensively revised Section 3.2, the classification is now entirely driven by quantitative physical metrics and statistically validated:

(1) Quantitative topological clustering (Text S2): Instead of subjective grouping, the 20 identified specific L-J weather types were aggregated into four major archetypes strictly based on their shared physical topology. We have added a new section (Text S2) in the Supplementary Material that explicitly lists the definitive, quantitative criteria used for this clustering: specifically relying on the polarity of SLP anomalies, the sign of geostrophic vorticity, and the primary azimuth of the geostrophic wind vectors. This ensures the classification rule is completely objective, transparent, and reproducible.

(2) Statistical validation via ANOVA (Fig. 6 & Table S2): To quantitatively prove that these four clustered archetypes are not arbitrary but represent fundamentally distinct atmospheric environments, we performed a One-Way Analysis of Variance (ANOVA). As explicitly added in Section 3.2, we calculated the nocturnal anomalies (Δ) of key micro-meteorological variables (T, RH, WS, PBLH, and U^*) across the four groups. The ANOVA results (all $p < 0.01$) provide definitive statistical proof that our classification algorithm objectively isolates completely different boundary layer thermodynamic structures.

(3) Direct evidence of high-altitude consistency (Fig. S5): Furthermore, to prove that this surface-based classification effectively captures broader synoptic forcing, we generated a new figure (Fig. S5). This explicitly demonstrates that the SLP gradients governing our categories perfectly align with the 850 hPa geostrophic wind flows across all identified types.

Lines 259-263:

Furthermore, to explicitly validate that this SLP-based classification accurately captures airflow characteristics in lower troposphere, Fig. S5 illustrates the spatial distributions of mean SLP overlaid with 850 hPa wind fields for the 20 identified weather types. The spatial patterns demonstrate a high degree of physical consistency, wherein the surface pressure gradients align with the 850 hPa wind field. This confirms that the SLP-based Lamb-Jenkinson method is highly robust and effectively represents synoptic circulation background of upper boundary-layer.

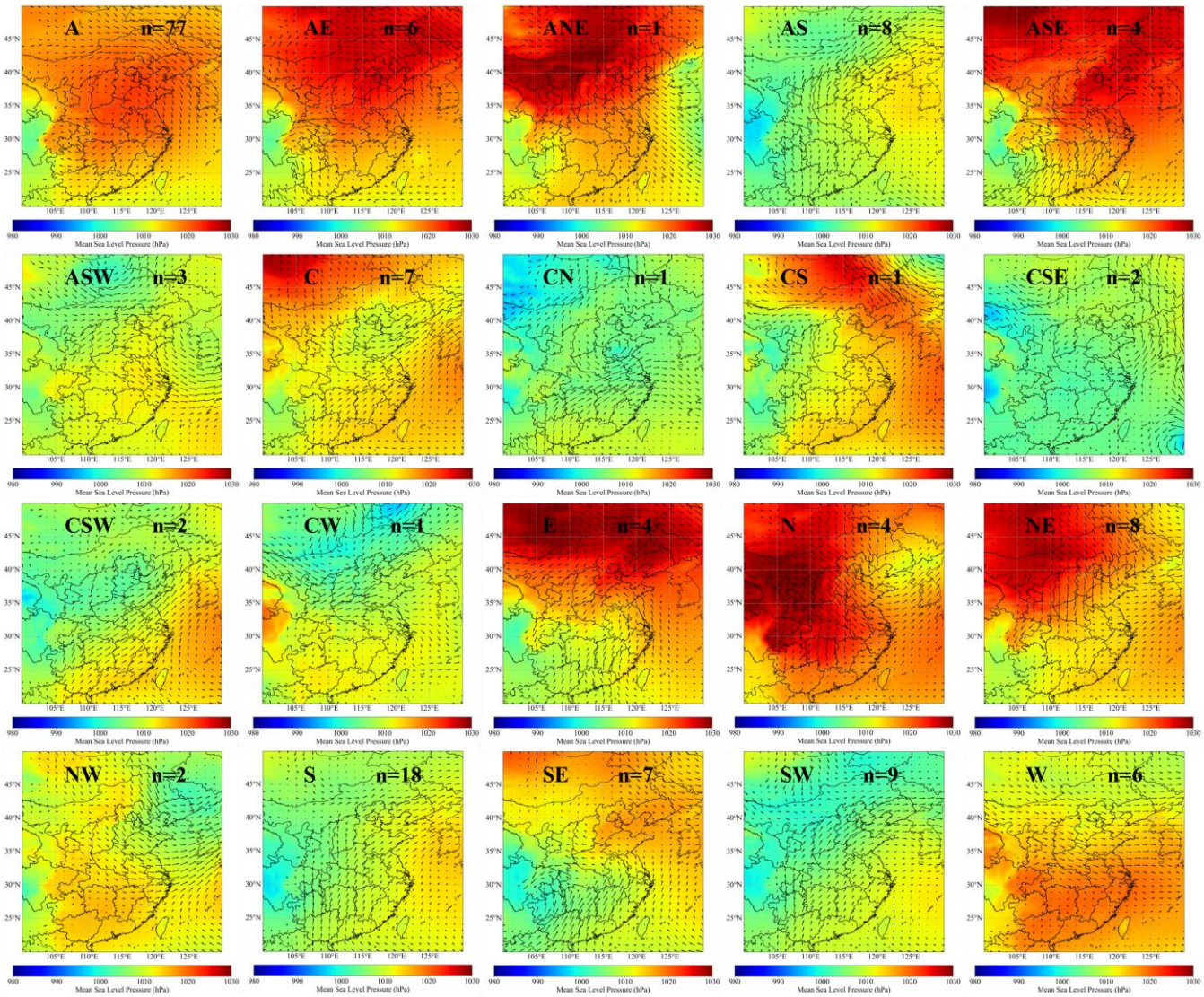

Figure S5: Spatial distribution of composite mean SLP and 850 hPa wind fields under different weather types (Preliminarily identified based on the Lamb-Jenkinson synoptic circulation classification method; n denotes the number of days).

Lines 276-296:

Notably, to extract the overarching dynamical mechanisms and reduce the statistical noise of the 20 specific Lamb-Jenkinson weather types, we quantitatively clustered them into four major archetypes: Anticyclonic (A-type), Cyclonic (C-type), Southerly (S-type), and West-North-East (WNE-type). Rather than subjective grouping, this clustering was rigorously based on their shared physical topology: specifically, the polarity of SLP anomalies, geostrophic vorticity, and the primary azimuth of geostrophic wind vectors. The detailed quantitative criteria for each of the four weather types are provided in Text S2. To further validate the physical distinctness of this

categorization, composite analysis of the synoptic fields and Analysis of Variance (ANOVA) on localized boundary layer variables were conducted.

To verify that the four grouped weather types possess fundamentally distinct atmospheric backgrounds, we analyzed their composite mean SLP and 850 hPa wind fields (Fig. 5). The spatial distributions unequivocally demonstrate distinct synoptic forcings: A-type is dominated by a strong, uniform high-pressure center over the study region (Fig. 5(a)); C-type is characterized by cyclonic curvature and low-pressure system (Fig. 5(b)); S-type is driven by intense southerly advection between a western low and an eastern high (Fig. 5(c)); and WNE-type features strong northeasterly flows driven by a massive continental high to the northwest (Fig. 5(d)). Furthermore, to statistically confirm that these different synoptic structures translate into distinctly different local thermodynamic environments, a One-Way ANOVA was performed on the nocturnal anomalies of key meteorological variables (T, RH, WS, PBLH and U^*) across the four groups. The resulting statistical distributions and data spreads are visually compared in Fig. 6, while the precise quantitative parameters and significance test results are detailed in Table S2. To strictly isolate the meteorological perturbations driven by synoptic systems and to eliminate the influence of seasonal and interannual backgrounds, the nocturnal anomalies (Δ) for key meteorological variables were calculated as the difference between the NOI days' specific nocturnal average and the corresponding monthly nocturnal mean. The results show that the inter-group differences are highly statistically significant (all $p < 0.01$), definitively proving that our quantitative classification objectively separates fundamentally different boundary layer environments.

Text S2: Quantitative grouping criteria.

(1) A-type (Anticyclonic group): This category quantitatively lumps all subtypes characterized by strong anticyclonic vorticity and positive SLP anomalies dominating the North China Plain (e.g., Pure A, and hybrid A types like AE, AW). Physically, these are unified by their shared capacity to induce broad regional subsidence.

(2) C-type (Cyclonic group): This lumps subtypes dominated by cyclonic vorticity and negative SLP anomalies (e.g., Pure C, and hybrid C types), unifying them through their shared dynamic triggering of localized convective downdrafts or atmospheric instability.

(3) S-type (Southerly group) & WNE-type (West-North-East group): The directional types

were categorized quantitatively based on the dominant azimuth of the geostrophic wind vectors and the strong orientation of the pressure gradient force, representing distinct horizontal advection and shear-induced mixing profiles.

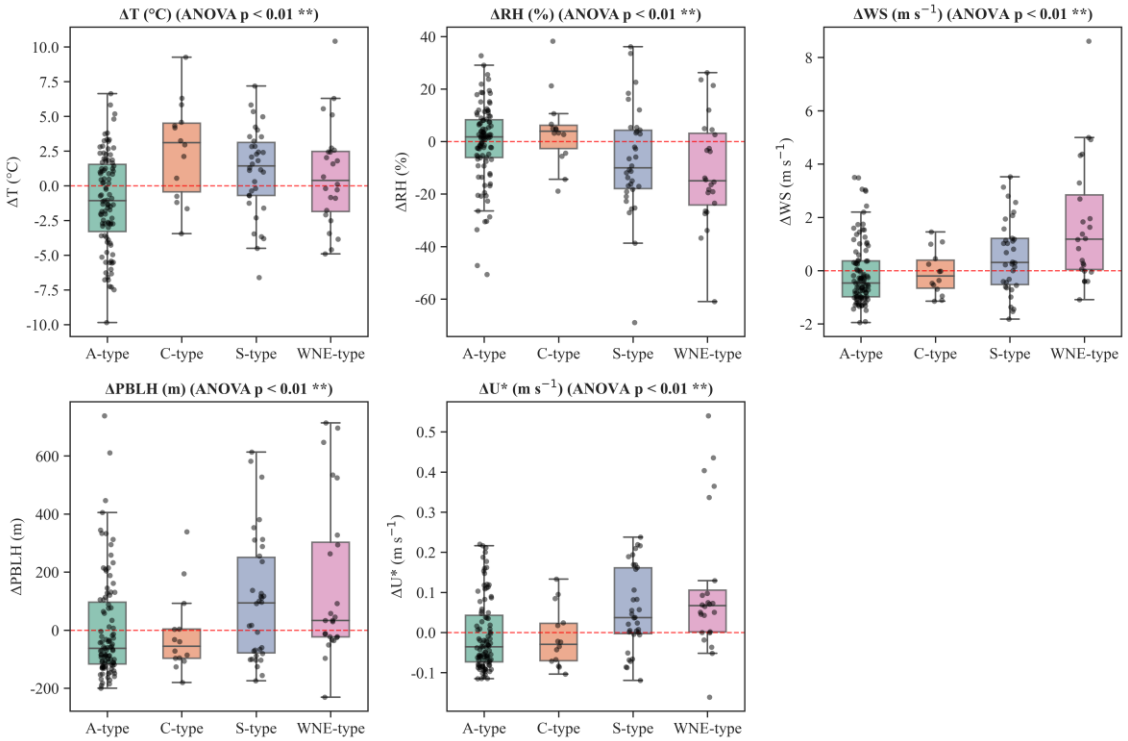

Figure 6: One-way ANOVA results for key meteorological variables (T, RH, WS, PBLH and U^*) of different synoptic categories. In each boxplot, the central black solid line indicates the median. The horizontal red dashed line denotes the zero-anomaly reference.

Table S2. Statistical summary of nocturnal meteorological anomalies and ANOVA results under the four weather types.

Variable	A-type	C-type	S-type	WNE-type	p-value
ΔT (°C)	-1.07 ± 3.41	2.60 ± 3.54	1.06 ± 3.18	0.77 ± 3.70	$< 0.01^{**}$
ΔRH (%)	-0.31 ± 14.82	4.08 ± 14.00	-7.12 ± 20.46	-11.15 ± 20.72	$< 0.01^{**}$
ΔWS (m s^{-1})	-0.10 ± 1.21	-0.08 ± 0.83	0.54 ± 1.39	1.74 ± 2.32	$< 0.01^{**}$
ΔPBLH (m)	3.56 ± 178.15	-14.44 ± 139.19	102.41 ± 216.82	156.22 ± 274.82	$< 0.01^{**}$
ΔU^* (m s^{-1})	-0.01 ± 0.09	-0.01 ± 0.07	0.06 ± 0.10	0.11 ± 0.17	$< 0.01^{**}$

Note: Data are presented as Mean ± Standard Deviation. The anomalies (Δ) were calculated relative to their respective monthly nocturnal means. The p-values are derived from One-Way ANOVA tests indicating statistical significance under the four weather types.

5. The measurement stations are not described. When presenting NOI statistics by station, the surrounding environment of each site is essential context. If a station is located near NO_x sources, the ozone signal will be titrated, and any observed increase will be attenuated or masked. Without characterizing the local emission environment, it is impossible to assess whether the detected NOIs are genuinely representative of mesoscale transport or simply artefacts of local source variability from the preceding hours.

Response 5: Thanks for reviewer's comments. To clarify the representativeness of our stations, we have detailed the environmental context of the measurement sites in the revised manuscript (Section 2.1). We respectfully provide the following two robust justifications to confirm that the observed NOI represent synoptic forcing:

(1) The nature of urban stations (Section 2.1): We clarified in the revised manuscript that all four measurement sites (KF, DY, XY, DX) are officially classified as national "urban evaluation sites" (which serve as urban stations) located within the built-up areas of Xinxiang. According to national siting criteria, these stations are specifically positioned to avoid direct, isolated micro-scale point sources (e.g., immediate traffic arteries or industrial facilities). Consequently, they share a consistent urban typology and experience comparable baseline NO titration sinks. This consistency minimizes the risk of severe, localized titration artifacts masking the regional signal.

(2) The rigorous simultaneous occurrence filter (Section 2.3): More importantly, as stated in Section 2.3, to completely rule out the possibility that the detected events are artefacts of local source variability, our study strictly filtered and focused only on representative NOI days where the O_3 surge occurred simultaneously across all different stations. A highly localized emission anomaly or a sudden drop in local NO_x at one specific street corner cannot physically trigger an identical, simultaneous O_3 surge across four geographically separated stations. These simultaneous occurrences serve as undeniable evidence of synoptic forcing (such as boundary-layer subsidence or regional advection).

Lines 91-99:

It is important to note that all four stations are officially classified as urban evaluation sites located within the urban areas of Xinxiang. In this study, these four stations were deliberately selected due to their strong spatial representativeness over the urban core and their high data completeness. Because these stations share a consistent urban typology, they experience highly

comparable baseline chemical environments (e.g., similar baseline nitrogen monoxide (NO) titration sinks and anthropogenic precursor availability). This spatial consistency is a crucial methodological design: it effectively minimizes random micro-scale chemical biases and isolated emission noise. By strictly controlling for these localized chemical heterogeneities, we ensure that the concurrent NOI events captured by this network genuinely reflect the overarching regional synoptic forcing and its subsequent, synchronized mechanical disruption of the local boundary layer, rather than random chemical artifacts.

Lines 234-242:

It is worth noting that non-overlapping NOI events frequently occur among the different stations, highlighting the inevitable influence of random localized emission noise and uncoordinated micro-environmental fluctuations. To rigorously isolate the overarching synoptic-scale meteorological drivers from these random local chemical/emission noises, this study specifically focused on representative events where NOI occurred simultaneously across all stations. Rather than dismissing local boundary-layer processes, these simultaneous occurrences serve as robust indicators of powerful regional episodes. They demonstrate that the large-scale synoptic forcing was sufficiently intense to synchronize the local boundary-layer dynamics (e.g., vertical wind shear and turbulent mixing) across the entire urban region. This rigorous screening ensures that the localized physical mechanisms evaluated in subsequent sections are systematically driven by macro-weather types, rather than coincidental local perturbations.

6. The rationale for selecting 850 hPa in Figure 3 is not provided in the methodology, and the wind scale is missing from the figure.

Response 6: Thanks for reviewer's comments. We have addressed both points in the revised manuscript:

(1) Rationale for 850 hPa: We have added an explicit justification to the Methodology section (Section 2.1). The revised text now explains: "Notably, the 850 hPa pressure level (approximately 1500 m above ground level) was specifically selected for the spatial wind field analysis. Because this altitude generally resides just above the planetary boundary layer, the airflow is largely free from localized surface friction and complex topographic disturbances. Consequently, it serves as the

most representative level for identifying mesoscale horizontal advection, low-level jets, and regional synoptic transport pathways that drive O_3 redistribution."

(2) Missing wind scale: We have now updated the figures (e.g., Fig. 7) to include a standard reference wind vector scale (→ 10 m s^{-1}) in each panel to accurately quantify the geostrophic wind arrows, alongside the existing color bar for absolute wind speed.

Lines 110-114:

Notably, the 850 hPa pressure level (approximately 1500 m above ground level) was specifically selected for the spatial wind field analysis. Because this altitude generally resides just above the planetary boundary layer, the airflow is largely free from localized surface friction and complex topographic disturbances. Consequently, it serves as the most representative level for identifying mesoscale horizontal advection, low-level jets, and regional synoptic transport pathways that drive O_3 redistribution.

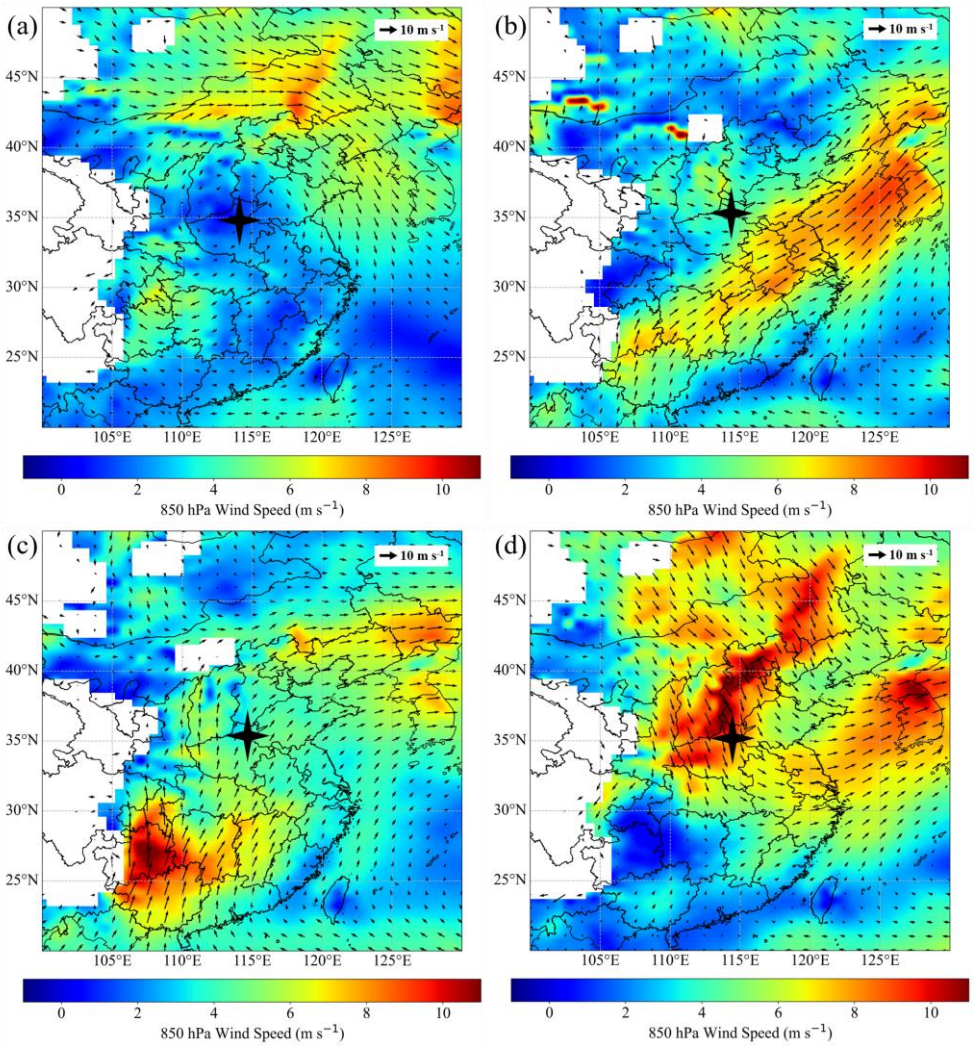

Figure 7: Spatial distribution of wind field at 850hPa under different weather types: (a) A-type, (b) C-type, (c) S-type, (d) WNE-type (asterisk indicates the location of Xinxiang).

7. Vertical profile data sources are not identified. When vertical profiles are discussed, no information is given about the data origin. The wind legend in Figure 5 is also incomplete.

Response 7: Thanks for reviewer's comments. We have revised relevant text in manuscript:

(1) Vertical profile data sources: The specific data origin and resolution for the vertical profiles were detailed in the Methodology (Section 2.1), where we stated that the "17-layer vertical profiles (500-1000 hPa)... were acquired from the Modern-Era Retrospective Analysis for Research and Applications dataset (MERRA-2)."

(2) Incomplete wind legend: This figure (revised Fig. 10) mainly illustrates vertical airflow characteristics (upward and downward motions) over Xinxiang. The sign of vertical pressure velocity directly indicates airflow direction: positive values represent downward motion, while negative values correspond to upward motion. Accordingly, we have removed the redundant wind vector arrows from the figure.

Lines 99-103:

Sea level pressure (SLP) data and 17-layer vertical profiles (500-1000 hPa) of vorticity, wind speed (WS), wind direction, temperature (T), relative humidity (RH) and O_3 concentration were acquired from the Modern-Era Retrospective Analysis for Research and Applications dataset (MERRA-2, Version 2, with a spatial resolution of 0.5° × 0.625° and temporal resolutions of 1 hour for surface data and 3 hours for 3D vertical profiles) (https://disc.gsfc.nasa.gov/).

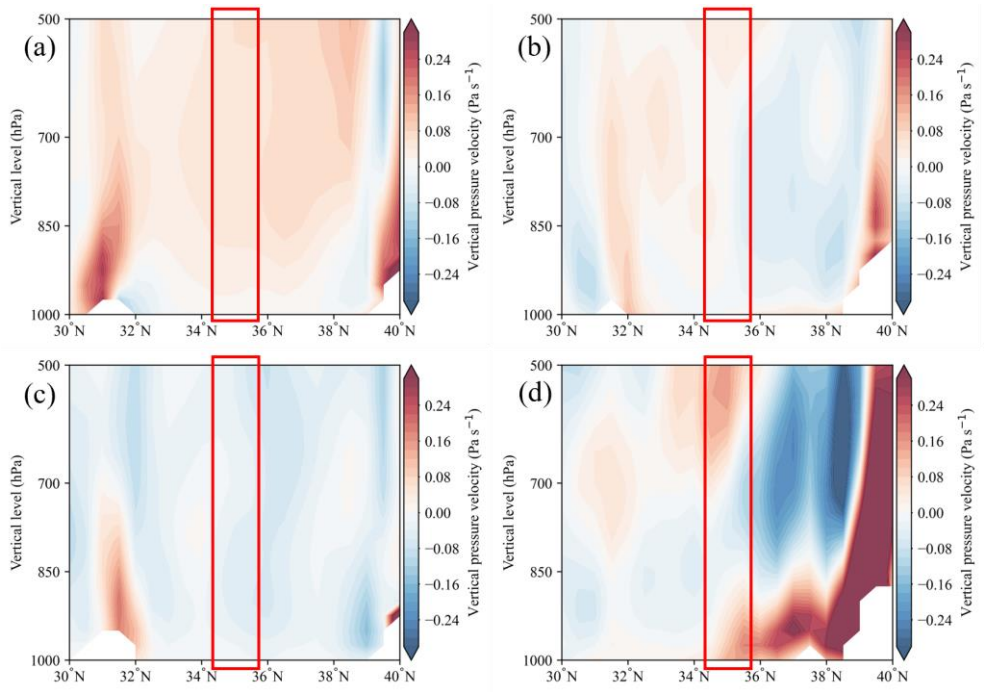

Figure 10: Vertical profiles of pressure velocity under different weather types: (a) A-type, (b) C-type, (c) S-type, (d) WNE-type (red rectangles indicate the region of Xinxiang). In terms of vertical pressure velocity, negative values correspond to upward motion, while positive values indicate subsidence.

Results and Interpretation:

1. The finding that most NOI events occur between March and September adds no new knowledge. This is simply when background ozone concentrations are highest, and the result follows trivially from that fact.

Response 1: Thanks for reviewer's comments. March to September is indeed the period with the highest background O_3 concentrations due to intense daytime photochemistry. At first glance, the seasonality of NOI does appear to perfectly mirror this background trend.

This phenomenon made us realize a flaw in our original narrative: we failed to clearly articulate the fundamental physical distinction between a passive photochemical background and an active dynamic intrusion. Inspired by reviewer's comment, we have introduced a "Reservoir vs. Trigger" paradigm in the revised manuscript to explicitly demonstrate why this seasonal finding is far from trivial:

(1) The reservoir (high background): The warm season builds up a large O_3 reservoir aloft. Within the nocturnal boundary layer, intense NO titration occurs. Even with extremely high

daytime O_3 levels, surface O_3 concentration declines rapidly at night. By contrast, O_3 in the residual layer is barely affected by titration and thus maintains high concentrations persistently.

(2) The trigger (active physical forcing): At night, O_3 cannot be produced via photochemical reactions, so its concentration rise is solely driven by physical transport. Although the residual layer holds abundant O_3 reservoirs in the warm season, the high-concentration O_3 can reach the surface and trigger NOI events when strong meteorological mechanical triggers (e.g., intense wind shear and prominent anticyclonic subsidence) break through the inversion layer and drive downward transport. Furthermore, strong NO titration occurs near the surface at night. The emergence of NOI also requires overcoming O_3 loss caused by titration to achieve a net increase in O_3 concentration.

(3) Clarifications in the revised text: To dispel the potential misconception that NOI is a passive byproduct of high backgrounds, we have expanded Section 3.1.1. We explicitly state: "While the warm season provides a highly concentrated aloft reservoir, the actual occurrence of an NOI event (which must vigorously overpower the intense local nocturnal NO titration) strictly requires the concurrent presence of specific dynamic meteorological triggers."

By explicitly separating the photochemical availability of the reservoir from the meteorological triggers (the core focus of this study), we believe the non-trivial nature and scientific value of these dynamic transport events are now robustly established.

Lines 194-197:

However, it is crucial to emphasize that a high regional O_3 background does not trivially dictate the occurrence of NOI. While the warm season provides a highly concentrated aloft reservoir, the actual occurrence of an NOI event (which must vigorously overpower the intense local nocturnal NO titration typical of urban environments) strictly requires the concurrent presence of specific dynamic meteorological triggers.

2. The role of calm conditions versus high wind speeds is not sufficiently interrogated. While the results suggest a higher frequency of NOI under calm conditions, events are also identified under elevated wind speeds. These cases could reflect fumigation from elevated layers, or transport associated with pre-frontal air masses carrying accumulated pollution that is subsequently scavenged after frontal passage — a mechanism already documented in the literature. This alternative explanation is not discussed.

Response 2: Thanks for reviewer's comments. We have completely rewritten Section 3.3 in the revised manuscript to shift the focus from descriptive seasonal meteorology to rigorous boundary-layer mechanical forcing. Following reviewer's expert suggestion, the revised text now rigorously contrasts these scenarios:

(1) Interrogating calm conditions (A-type): We now explicitly characterize A-type as pure synoptic subsidence occurring under extremely calm conditions. As added to the revised text, the negative anomalies in local wind speed and friction velocity confirm a highly stable environment. Here, the trigger is macro-scale subsidence pushing against the inversion.

(2) Interrogating elevated wind speeds (WNE-type): Under WNE-type, we found high wind speeds (mean: $\Delta WS = 1.74$ m s^{-1}) and intense turbulent mixing (mean: $\Delta U^* = 0.11$ m s^{-1}). In the revised text, we have explicitly linked this observed intense mechanical downward mixing with the nocturnal "fumigation-like processes" documented in the literature.

Lines 323-329:

Under A-type, Xinxiang was located near a high-pressure center, with an outward-rotating wind field at 850 hPa (Figs. 5(a) and 7(a)), indicating the presence of an anticyclonic high-pressure system. Driven by this synoptic forcing, Xinxiang experienced extremely calm conditions. As explicitly demonstrated by the nocturnal anomalies in Fig. 6 and Table S2, A-type was characterized by negative anomalies in wind speed (mean: $\Delta WS = -0.10$ m s^{-1}) and friction velocity (mean: $\Delta U^* = -0.01$ m s^{-1}), alongside a strongly constrained boundary layer (mean: $\Delta PBLH = 3.56$ m, representing negligible expansion). This indicates that the overriding high-pressure system creates a highly stable environment. The explicit intrusion process of O_3 under this subsidence will be further verified in Section 3.4.

Lines 351-367:

Although Xinxiang often featured a massive continental high-pressure system (e.g., the Siberian High) to the northwest under WNE-type (Fig. 5(d)), their local dynamics are fundamentally different from the pure subsidence of A-type. At 850 hPa, the region was obviously influenced by a northwestern airflow (Fig. 7(d)), consistent with the geostrophic wind characteristics of WNE-type. Unlike A-type, where the study area sits calmly at the high-pressure center, under WNE-type, Xinxiang was located at the densely packed periphery of the advancing

high. Consequently, the macroscopic forcing shifts to intense horizontal pressure gradients (Figs. 5(d) and 7(d)). This kinematic distinction is perfectly captured by the localized surface anomalies (Table S2). WNE-type exhibited the most extreme positive anomalies among all categories, with local wind speed (mean: ΔWS = 1.74 m s^{-1}) and friction velocity (mean: ΔU^* = 0.11 m s^{-1}) far exceeding other types. Driven by this intense horizontal advection and wind shear, the nocturnal boundary layer experienced massive mechanical lifting (mean: $\Delta PBLH$ = 156.22 m). Furthermore, this intense mechanical mixing effectively breaks the nocturnal surface inversion, bringing slightly warmer air from aloft downward (detailed mechanism analysis is presented in Section 3.4.2). This vigorous downward mixing of the elevated residual layer shares conceptual similarities with the nocturnal fumigation-like processes documented in other literature (Wu et al., 2023; He et al., 2022), which also explains the observed positive temperature anomaly (mean: ΔT = 0.77 °C). Therefore, despite the high-pressure background, it is this extraordinarily strong localized shear and turbulent mixing, that serves as the primary mechanical driver forcing O_3 downward to the surface during WNE-type. Combined with rapid dispersion of local NO emissions under high winds that greatly mitigates nighttime titration, vigorous vertical entrainment counteracts both horizontal diffusion and titration loss of O_3, and ultimately causes a net O_3 surge.

3. The WNW weather type results are likely of limited ozone relevance. High wind speeds under this type are typically associated with enhanced dispersion, making it doubtful that these events represent meaningful ozone loading.

Response 3: Thanks for reviewer's comments. High wind speeds generally act as a diluting agent, which typically reduces the surface loading of primary pollutants (e.g., NO_x or CO). Under normal daytime conditions, this logic perfectly applies to O_3 as well.

Inspired by reviewer's comment, we recognized that our original manuscript failed to elaborate the physical effects of unique strong wind events within the nocturnal boundary layer. For nighttime O_3, strong winds associated with the WNE circulation pattern activate a coupled physical and chemical mechanism:

(1) Dispersion of the chemical sink (rather than the O_3 source): At night, O_3 in the urban surface layer is rapidly consumed via intensive NO titration, whereas abundant O_3 accumulates within the elevated residual layer aloft. Accordingly, near-surface strong winds exert far weaker

dilution effects on the scarce surface O_3 than they do during daytime. Meanwhile, such strong winds swiftly transport and dilute high-concentration local primary pollutants at night, mainly nitric oxide (NO). The rapid dilution of NO greatly weakens the dominant chemical sink for nocturnal O_3.

(2) Intense mechanical downward entrainment: Concurrently, these high wind speeds generate powerful localized mechanical turbulence. As explicitly validated by our localized anomalies (detailed in the revised Section 3.3), the WNE-type triggers massive mechanical lifting of the boundary layer (mean: ΔPBLH = 156.22 m) and generates extremely high friction velocity (ΔU^* = 0.11 m s^{-1}). The powerful turbulence mixing entrains the O_3-rich air from the residual layer downward to the surface.

Relevant revised text in the manuscript is presented in Lines 351–367.

4. Line 249 mentions a thermal low-pressure system without discussing its potential influence on ozone dynamics, which is a notable omission given the likely relevance of this feature to the observed transport patterns.

Response 4: Thanks for reviewer's comments. Thermal low-pressure systems are highly relevant to regional O_3 dynamics, particularly regarding daytime accumulation and large-scale mass transport.

In the original manuscript, we briefly mentioned this daytime thermal low-pressure system merely in the context of general seasonal climatology. However, we realized that introducing a daytime thermal feature without rigorously linking it to the specific nocturnal intrusion mechanism created a disjointed narrative.

Because the core focus of this study is the dynamic triggering of nocturnal O_3 enhancements (NOI), the daytime thermal low-pressure system (while crucial for building the aloft O_3 reservoir) is not the direct mechanical driver that physically breaks the nocturnal surface inversion. Therefore, to resolve this omission and prevent any distraction from the core causal mechanisms, we took the following steps:

(1) Removal of disjointed daytime climatology: As part of our major structural overhaul of Section 3.3 (to refocus the manuscript strictly on nocturnal mechanical triggers), we have completely removed the descriptive paragraph regarding daytime seasonal climatology, including the isolated reference to the thermal low-pressure system.

(2) Exclusive focus on nocturnal transport drivers: Instead, the revised discussion of the S-type

transport pattern now focuses exclusively on the definitive nocturnal synoptic and boundary-layer drivers. Specifically, we now comprehensively discuss the nocturnal tight pressure gradients and their specific localized mechanical responses: significant positive anomalies in local wind speed (mean: $\Delta WS = 0.54$ m s^{-1}) and friction velocity (mean: $\Delta U^* = 0.06$ m s^{-1}), which lead to substantial nocturnal boundary layer lifting (mean: $\Delta PBLH = 102.41$ m).

We believe that by completely removing the disconnected daytime climatology and focusing entirely on these rigorous nocturnal mechanical metrics, the revised manuscript now provides a highly focused, dynamically sound interpretation of the S-type nocturnal transport patterns.

Lines 342-350:

S-type represents a dynamic environment driven by distinct horizontal advection. Under S-type, Xinxiang was situated in a tight pressure gradient, typically between a western low and an eastern high (Figs. 5(c) and 7(c)). Driven by this synoptic setup, continuous southerly geostrophic winds prevailed over the region. As detailed in Table S2, S-type produced significant positive anomalies in local wind speed (mean: $\Delta WS = 0.54$ m s^{-1}) and friction velocity (mean: $\Delta U^* = 0.06$ m s^{-1}). These specific values rigorously demonstrate that beyond facilitating regional horizontal transport (which will be explicitly traced in Section 3.4.1), the southerly advection directly generates substantial localized mechanical turbulence at the surface, physically lifting the nocturnal boundary layer (mean: $\Delta PBLH = 102.41$ m). This localized mechanical shear serves as the direct trigger for breaking nocturnal stability, subsequently entraining O_3-rich air from the elevated residual layer down to the surface and triggering NOI events.

5. The decoupling of weather type frequencies, ozone concentrations, and Figure 3 meteorology makes it impossible to assess the actual severity of the identified increases. A summary table integrating these dimensions would greatly improve readability and analytical clarity. As currently presented, the results section is difficult to follow.

Response 5: Thanks for reviewer's comments. The original results section was difficult to follow and that the meteorological drivers felt disjointed from the severity of the events.

To fundamentally resolve this issue, we have completely overhauled the narrative in Section 3.3. However, regarding the specific construction of the summary table, we encountered a fundamental atmospheric chemistry caveat that led us to refine reviewer's suggestion:

(1) The risk of confounding dynamic severity with chemical mass balance: We initially attempted to construct the integrated table coupling weather types directly with specific absolute O_3 mass increments. However, we realized this approach inadvertently obscured the true physical mechanism. As is well established, the observed nocturnal O_3 increment is an extremely complex mass-balance outcome (involving horizontal advection, vertical entrainment, and non-linear chemical titration by NO). Because the absolute O_3 surge is heavily confounded by the baseline daytime accumulation, directly coupling it with overarching weather types risks implying an oversimplified linear causality.

(2) Establishing Table S2 as the quantitative severity matrix: To maintain a strict scientific focus on the physical drivers while directly addressing a tabulated summary, we designated Table S2 (localized nocturnal meteorological anomalies) as our definitive diagnostic matrix. Instead of absolute chemical outcomes, Table S2 explicitly integrates and contrasts the intrinsic physical driving severity across all weather types (ΔWS, ΔU^*, ΔPBLH…). Since Figure 6 and Table S2 convey similar information, we place Figure 6 in the main text and Table S2 in the supplementary materials.

(3) Narrative coupling in the revised Section 3.3: Complementing Table S2, the narrative in the revised Section 3.3 is now strictly coupled. For each weather type, we immediately link the macro-scale synoptic forcing directly to these tabulated localized boundary-layer triggers (incorporating quantitative anomalies like T, RH, WS, U^* and PBLH).We believe that this mechanism-focused framework, anchored by Table S2 as the analytical benchmark, effectively resolves the readability issues and provides a clear integration of dimensions without oversimplifying the complex chemical mass balance of nocturnal O_3.

Relevant revised text in the manuscript is presented in Lines 307–367.

6. Supplementary figures are referenced repeatedly in the main text without adequate explanation.

Response 6: Thanks for reviewer's comments. To greatly improve the readability and ensure a smooth, self-contained narrative in the main text, we have conducted a comprehensive review of all supplementary citations and made the following major improvements in the revised manuscript:

(1) Expanding in-text interpretations: We have systematically gone through the manuscript and expanded the textual descriptions whenever a supplementary figure is cited. Instead of merely citing

the figure number, the revised main text now explicitly summarizes the key points and visual evidence provided by that specific supplementary figure, ensuring the reader understands the analytical point without strictly needing to open the supplementary file.

(2) Elevating critical data to the main text: Furthermore, we realized that some supplementary data were simply too critical to be left in the appendix. Accordingly, several key contents have been integrated into the main text.

Lines 213-214:

Therefore, we further analyzed the O_3 diurnal variations on NOI days categorized by their occurrence time across different seasons (Fig. 2).

Lines 231-233:

We established unified occurrence dates through cross-analysis of multi-station data (Fig. 3), and found that KF, XY, DX, and DY had 171 NOI days occurring on the same days during 2021-2023 in Xinxiang.

Lines 290-292:

The resulting statistical distributions and data spreads are visually compared in Fig. 6, while the precise quantitative parameters and significance test results are detailed in Table S2.

Lines 408-410:

To validate this process, we analyzed the vertical profiles of pressure velocity (Fig. 10), thermodynamic stability (Fig. S9), O_3 concentrations (Fig. S10), and surface turbulence metrics (Fig. 11).

7. The absence of summary tables makes the results section hard to navigate. Given the number of weather types and stations discussed, tabulated summaries are necessary.

Response 7: Thanks for reviewer's comments. To explicitly improve the navigation without introducing misleading causal attributions, we took the following comprehensive steps:

(1) Creating a highly standardized, predictable narrative pipeline (Sections 3.3, 3.4.1, and 3.4.2): Rather than relying on a simplified table, we fundamentally resolved the navigation issue by

completely overhauling the text to act as a structural table. We have standardized the narrative flow across Sections 3.3, 3.4.1, and 3.4.2. Now, for every single weather type, the reader is guided through an identical, highly predictable logical pipeline:

Triggering precondition: The macroscopic synoptic forcing.

3D origin: High-altitude regional backward trajectories proving the aloft reservoir.

Downward intrusion: Specific local vertical mixing metrics (e.g., CAPE, ΔU^*, and PBLH fluctuations) physically pulling the O_3 downward.

By stripping away disjointed seasonal climatology and adhering strictly to this identical, three-step causal framework for each weather type, the revised text allows readers to intuitively compare mechanisms across categories without getting lost.

(2) Optimizing the visibility and integration of existing diagnostic tables: We realized our original manuscript failed to effectively guide the reader to the existing summaries. We have now heavily integrated and signposted Table S1 (frequencies) and Table S2 (quantitative boundary-layer anomalies). By anchoring our standardized narrative much more smoothly to these comprehensive tables, the quantitative differences are now highly visible.

(3) Elevating critical data to the main text: We systematically reviewed the entire manuscript. To prevent the reader from constantly flipping between the main text and the supplement, we have elevated several critical pieces of information directly into the main manuscript, streamlining non-essential details into the appendices.

We believe these synergistic improvements (standardizing the narrative pipeline across Sections 3.3 and 3.4, alongside better leveraging robust existing tables) have drastically improved the analytical flow, making the Results section highly intuitive to navigate.

Relevant revised text in the manuscript is presented in Lines 307–451.

Conceptual and Terminological Issues:

1. Line 50: Discussing "formation mechanisms" in the context of nocturnal ozone is conceptually inconsistent. At night, photochemical ozone production is absent; the relevant process is titration by NO, not formation. The framing needs to be corrected.

Response 1: Thanks for reviewer's comments. In the strict context of atmospheric chemistry, the

word “formation” is intrinsically associated with photochemical production. Using it alongside nocturnal O_3 could indeed cause conceptual ambiguity and inadvertently mislead readers into thinking about chemical production.

To eliminate any potential for terminological confusion and to precisely reflect the true nature of these events, we have revised the manuscript and replaced “formation mechanisms” with “physical mechanisms”. The revised sentence in the introduction now reads: “While daytime O_3 pollution is well-documented, NOI remains poorly understood, necessitating the research into its meteorological drivers and physical mechanisms”.

Furthermore, to ensure absolute conceptual consistency throughout the entire manuscript and to highlight the physical nature of this research, we have systematically replaced “formation” with “physical mechanisms” or “physical transport” when discussing nocturnal events. We have even updated the title of the manuscript to reflect this precise mechanistic focus.

2. "Meteorological activities" (Line 49) is not standard scientific terminology and should be revised.

Response 2: Thanks for reviewer’s comments. Meteorological activities are not standard scientific terminology in this context. To ensure precise academic phrasing, we have revised the text and replaced it with “meteorological phenomena”. The revised sentence in the introduction now reads: “NOI events, usually driven by horizontal and vertical transport processes, are linked to meteorological phenomena such as sea-land winds (Nair et al., 2002), valley winds (Sánchez et al., 2005; Xue et al., 2023), low-level jets and convective storms (Zhu et al., 2020; Wu et al., 2023)”.